

Article

Influence of Defects and H₂O on the Hydrogenation of CO₂ to Methanol over Pt Nanoparticles in UiO-67 Metal-Organic Framework

Emil Sebastian Gutterød, Sri Harsha Pulumati, Gurpreet Kaur, Andrea Lazzarini, Bjørn Gading Solemsli, Anette Eleonora Gunnæs, Christian Ahoba-Sam, Maria Evangelou Kalyva, Johnny Andreas Sannes, Stian Svelle, Egill Skulason, Ainara Nova, and Unni Olsbye

J. Am. Chem. Soc., **Just Accepted Manuscript** • DOI: 10.1021/jacs.0c07153 • Publication Date (Web): 09 Sep 2020

Downloaded from pubs.acs.org on September 9, 2020

Just Accepted

"Just Accepted" manuscripts have been peer-reviewed and accepted for publication. They are posted online prior to technical editing, formatting for publication and author proofing. The American Chemical Society provides "Just Accepted" as a service to the research community to expedite the dissemination of scientific material as soon as possible after acceptance. "Just Accepted" manuscripts appear in full in PDF format accompanied by an HTML abstract. "Just Accepted" manuscripts have been fully peer reviewed, but should not be considered the official version of record. They are citable by the Digital Object Identifier (DOI®). "Just Accepted" is an optional service offered to authors. Therefore, the "Just Accepted" Web site may not include all articles that will be published in the journal. After a manuscript is technically edited and formatted, it will be removed from the "Just Accepted" Web site and published as an ASAP article. Note that technical editing may introduce minor changes to the manuscript text and/or graphics which could affect content, and all legal disclaimers and ethical guidelines that apply to the journal pertain. ACS cannot be held responsible for errors or consequences arising from the use of information contained in these "Just Accepted" manuscripts.

Influence of Defects and H₂O on the Hydrogenation of CO₂ to Methanol over Pt Nanoparticles in UiO-67 Metal-Organic Framework

Emil Sebastian Gutterød^a, Sri Harsha Pulumati^b, Gurpreet Kaur^a, Andrea Lazzarini^a, Bjørn Gading Solemsli^a, Anette Eleonora Gunnæs^c, Christian Ahoba-Sam^a, Maria Evangelou Kalyva^a, Johnny Andreas Sannes^a, Stian Svelle^a, Egill Skúlason^b, Ainara Nova^{d*} and Unni Olsbye^{a*}

^a Centre for Materials Science and Nanotechnology, Department of Chemistry, University of Oslo, Sem Sælandsvei 26, N-0315 Oslo, Norway.

^b Science Institute and Faculty of Industrial Engineering, Mechanical Engineering and Computer Science, University of Iceland, Hjarðarhagi 2, VR-III, 107 Reykjavík, Iceland.

^c Centre for Materials Science and Nanotechnology, Department of Physics, University of Oslo, Sem Sælandsvei 26, N-0349 Oslo, Norway.

^d Hylleraas Centre for Quantum Molecular Sciences, Department of Chemistry, University of Oslo, P.O. Box 1033, Blindern, N-0315 Oslo, Norway.

Abstract

In catalysts for CO₂ hydrogenation, the interface between metal nanoparticles (NPs) and the support material is of high importance for the activity and reaction selectivity. In Pt NP-containing UiO Zr-metal-organic frameworks (MOFs), key intermediates in methanol formation are adsorbed at open Zr-sites at the Pt–MOF interface. In this study, we investigate the dynamic role of the Zr-node and the influence of H₂O on the CO₂ hydrogenation reaction at 170 °C, through steady state and transient isotope exchange experiments, H₂O co-feed measurements and density functional theory (DFT) calculations.

The study revealed that an increased number of Zr-node defects increase the formation rates to both methanol and methane. Transient experiments linked the increase to a higher number of surface intermediates for both products. Experiments involving either dehydrated or prehydrated Zr-nodes showed higher methanol and methane formation rates over the dehydrated Zr-node. Transient experiments suggested that the difference is related to competitive adsorption between methanol and water. DFT calculations and microkinetic modeling support this conclusion and give further insight into the equilibria involved in the competitive adsorption process. The calculations revealed weaker adsorption of methanol in defective or de-hydrated nodes, in agreement with the larger gas phase concentration of methanol observed experimentally. The microkinetic model shows that [Zr₂(μ-O)₂]⁴⁺ and [Zr₂(μ-OH)(μ-O)(OH)(H₂O)]⁴⁺ are the main surface species when the concentration of water is lower than the number of defect sites. Lastly, although addition of water was found to promote methanol desorption, water does not change the methanol steady state reaction rate, while it has a substantial inhibiting effect on CH₄ formation. These results indicate that water can be used to

increase the reaction selectivity to methanol and encourages further detailed investigations of the catalyst system.

Introduction

The hydrogenation of CO₂ is receiving attention as a key reaction for sustainable production of fuels and value-added chemicals.¹⁻³ The activity and selectivity of CO₂ hydrogenation catalysts is strongly influenced by the nature of the metal-support interface.⁴⁻⁸ For Cu-based catalysts, the presence of ZrO₂ or isolated Zr moieties close to Cu facilitates methanol formation by forming low coordinated Lewis acidic Zr-sites, where formate and methoxy groups form in the presence of CO₂ and H₂.⁹⁻¹¹ Formate and methoxy groups are also observed at sites at the interface of Cu/Al₂O₃: at 4-coordinated sites, methanol forms from bidentate CO₂ bridged between two sites, via formate, while at 3-coordinated sites, CO formation from monodentate CO₂ is favored.¹² On Pt/Al₂O₃, it has been proposed that CO forms from carbonate-type intermediates on defective Al sites at the interface, either by O-abstraction by hydrogen, or by the filling of an oxygen vacancy.¹³

Studies of the CO₂ hydrogenation reaction to methanol over metal functionalized metal-organic frameworks (MOFs) have also brought further evidence of interactions between the nanoparticles (NPs) and the support material.¹⁴⁻¹⁸ Focusing here on the UiO-series of MOFs, they consist of 12-coordinated Zr₆O₄(OH)₄ nodes connected by e.g. benzene-1,4-dicarboxylic acid linkers (BDC; UiO-66) or biphenyl-4,4'-dicarboxylic acid linkers (BPDC; UiO-67), forming 3-dimensional, porous frameworks with fcc structure.

X-ray photoelectron spectroscopy (XPS) performed on Cu NPs at the UiO-66 surface showed evidence of Zr reduction in the presence of Cu, suggesting an interaction between the Cu NPs and the UiO-66 Zr-node.¹⁴ Furthermore, An *et al.* reported XPS evidence of Zr reduction in CuZn@UiO-67 with 100% bipyridine type linkers, and proposed that the reaction proceeds by CO₂ adsorption at unsaturated Zr-sites followed by H-spillover from Cu to the Zr-node.¹⁵

In two recent contributions from our group, we reported the CO₂ hydrogenation performance of an exceptionally stable MOF-based catalyst, consisting of Pt nanoparticles (NPs) *in-situ* formed in the cavities of UiO-67, herein called “UiO-67-Pt”. The first contribution focused on stability issues,¹⁶ while the second focused on catalyst performance and mechanistic studies.¹⁷ A performance comparison was carried out between UiO-67-Pt and Pt/C, Pt/SiO₂ and Pt/Al₂O₃ catalysts. The study showed that Pt/C and Pt/SiO₂ produced only CO, while Pt/Al₂O₃ produced mainly CO and a modest amount of methane and methanol (< 10 % selectivity to each of methane and methanol) at 170 °C, 1-8 bar, H₂/CO₂ = 6. On the other hand, UiO-67-Pt formed substantial amounts of methanol (up to 18 % selectivity), smaller amounts of methane (up to 2 % selectivity), and CO as majority product, under the same conditions. Combining steady state and transient kinetic methods revealed that methanol is formed from CO₂ via formate intermediates at open Zr-sites at the interface between the Pt NP and the

Zr-node. The study further showed that methanol is mechanistically separated from the byproducts, methane and CO, and that methane is formed mainly via CO, on this catalyst.¹⁷

In the current study, focus is set on the dynamic role of the Zr-node in UiO-67-Pt during the CO₂ hydrogenation reaction. We investigate the influence of the amount of defective open Zr-sites (i.e. sites not coordinated to linker molecules) on the formation of all three carbon-containing reaction products: methanol, methane and CO. Moreover, we employ steady state and transient water co-feed experiments, involving isotope labeling and DFT calculations, to gain insight into the role of node-hydration and influence of water in the reaction. The study shows a positive correlation between the number of node defects and the number of surface intermediates leading to methanol and methane formation, while it has a minor influence on CO formation. Furthermore, water co-feed was found to promote desorption of methanol, while it is detrimental to the formation of methane. These findings provide important leads to further catalyst and process design.

Experimental Details

The sample of UiO-67 was prepared by the procedure reported in ref. ¹⁷: in brief, a solution of ZrCl₄ (1 eq.), distilled water (6 eq.) and dimethylformamide (DMF) (50 eq.) was heated to 80 °C, and benzoic acid (3 eq.) was added. When the benzoic acid (BA) was dissolved, 2,2'-bipyridine-5,5'-dicarboxylic acid (BPYDC) (0.1 eq.) and 1,1'-biphenyl-4,4'-dicarboxylic acid (BPDC) (0.9 eq.) were added, and the resulting solution was heated under stirring overnight at 130 °C. The resulting MOF was washed with hot DMF and acetone, and then dried overnight (in air) at 150 °C. This sample is referred to as UiO-67.

To produce a sample with less missing linker defects, a BPDC healing procedure (modified from literature)¹⁹ was performed: 5 grams of the UiO-67 sample, pre-dried at 200 °C was dispersed in 100 ml DMF at 100 °C. BPDC (0.6 g) was added to the solution in order to replace the BA in UiO-67 (12.5 % with respect to BPDC, *vide infra*) with BPDC. After heating the solution at 100 °C overnight, the resulting powder was washed with DMF and acetone as above. This sample is referred to as UiO-67(LD).

Both MOF samples were impregnated with Pt following the procedure reported in ref. ¹⁶: K₂PtCl₄ corresponding to a 2:1 BPYDC:Pt molar ratio was added to the MOFs dispersed in DMF at 100 °C under stirring and left overnight. After washing in hot DMF and acetone, this leads to the formation of well-defined BPYDC-PtCl₂ moieties (where the BPYDC is in the MOF framework).^{20, 21}

For Pt/ZrO₂, ZrO₂ particles were prepared by a modified literature procedure.²² 2.15 g of ZrO(NO₃)₂.xH₂O (99 %, supplied by Sigma-Aldrich) was dissolved in 100 ml type 2 water and heated to 70 °C under reflux, followed by a dropwise addition of 100 ml of 0.3 M (NH₄)₂CO₃ (ACS Reag. Ph. Eur grade, from Merk KGaA) aqueous solution under stirring. After 2 h of stirring, the resulting

mixture was cooled to ambient temperature, centrifuged and then washed twice with type 2 H₂O. The resulting paste was oven-dried at 110 °C for 12 h and then calcined in air at 500 °C for 3 h. The calcined ZrO₂ was impregnated with 0.5 wt % Pt following the same procedure as for the MOF samples. Powder X-ray diffractograms of the MOFs were acquired using a Bruker D8 Discover instrument (Cu K α) with a Lynx Eye silicon detector. N₂ adsorption isotherms were measured at 77 K (BELSORP mini-II) after heating the samples under vacuum for 1 hour at 80 °C then 4 hours at 150 °C. After dissolving the samples in 1M NaOH/D₂O, solution state proton nuclear magnetic resonance (¹H-NMR) was utilized to determine the relative amounts of organic species in the MOFs. Thermogravimetric analysis was performed on a Netzsch STA 449 F3-Jupiter instrument. The samples (~20 mg) were heated to 800 °C in an Al₂O₃ sample holder under flow of 20 ml min⁻¹ 20 % O₂/N₂. A Hitachi SU8230 field emission scanning electron microscope (FESEM) with an XFlash 6|10 energy-dispersive X-ray (EDX) detector was used to estimate the Pt/Zr ratio of the two samples. The Pt/Zr ratio in the two samples were equal within the experimental accuracy (0.042 \pm 0.002 and 0.043 \pm 0.003 for UiO-67-Pt and UiO-67(LD)-Pt, respectively). Scanning transmission electron microscopy (STEM) images of UiO-67(LD)-Pt after activation and testing was acquired with a FEI Titan G2 60-300 kV microscope.

Most catalytic tests were performed in a fixed bed flow test setup with a stainless-steel reactor (I.D. 7 mm) where the effluent gas is analyzed by an on-line MS (Pfeiffer) and a GC (TCD-FID). Prior to catalytic testing, the materials were activated at 350 °C (5 °C min⁻¹ ramp and 4 hours isotherm) in flow of 10 % H₂/Ar (40 ml min⁻¹). The catalysts (0.2 g) were tested in 1/3/1 and 1/6/3 CO₂/H₂/Ar flow (τ = 0.01 g_{cat} min ml⁻¹) under 1 and 8 bar pressure, at 170 °C. Pre-hydration, H₂O co-feed, and ¹³CO₂/¹²CO₂ SSITKA (Steady-State Isotope Transient Kinetic Analysis) experiments were performed and the details are reported in-text.

The high-pressure catalytic tests were performed using a Microactivity Effi unit built by PID Eng & Tech (Micromeritics). The unit is equipped with a high-speed servo-controlled needle valve which allows for precise and stable control of pressure from 1 to 100 bar. A stainless steel flow reactor (6 mm I.D) was used for the tests. The catalysts were activated at 350 °C (5 °C/min ramp) for 4 h in 10 % H₂ in inert (10 % Kr in Ar) flow prior to the testing. The catalysts (0.2 g) were tested with 1/6/3 CO₂/H₂/inert flow ratios (τ = 0.01 and 0.02 g_{cat} min ml⁻¹ for the UiO-67-Pt and Pt/ZrO₂ samples respectively) aimed at similar CO₂ conversions within 1-30 bar, and 170 -240 °C. The effluent from the reactor was analysed with an online GC (Agilent 8890 equipped with one TCD and 2 FIDs, with a methanizer coupled to one of the FIDs to analyse both CO_x and oxygenates on one column using one detector).

Computational Details

For the computational study, all chemical species were optimized using DFT calculations with a mixed Gaussian and plane wave method (GPW)²³⁻²⁵, as implemented in CP2K-6.1 version^{26, 27}. We used PBE-D3 functional^{28,29} with Gaussian basis set DZVP-MOLOPT-SR-GTH^{30,31}. A multigrid of size 5 was used to map the Gaussian basis functions, with cut-off energy of 360 Ry for plane wave basis. Energy barriers were calculated using the climbing image nudged elastic band (CI-NEB) method^{32,33}. Micro Kinetic model is built with COPASI.³⁴ Further details on the calculations are given in Supporting Information (SI).

In our previous study¹⁷ we concluded that the active site for methanol formation are the Zr-nodes of the UiO-67 system. In this work, the reactivity of the Zr-sites active towards the reaction products CH₃OH and H₂O, was explored in more detail. To decrease the computational cost of the overall study we constructed a simple model where the UiO-67 framework optimized from our previous work¹⁷ is stripped to a single zirconium node with twelve benzoate linkers, as shown in Figure 1(a). To maintain the structure of the MOF and better simulate the real configuration of the catalyst, carbon atoms at the end of the linkers were constrained in all directions to prevent the node from deforming and maintaining the integrity of the MOF. One linker was removed from the model in Figure 1(a) to simulate a missing linker defect as shown in Figure 1(b). This system is used to investigate the equilibrium between methanol and water desorption. Two linkers were also removed from the original 12 linkers model system to create either the two adjacent missing linker defects in Figure 1(c) or two opposite missing linker defects in Figure 1(d). The one linker and two linker defect systems were used to model the UiO-67(LD) and the UiO-67 systems, respectively. This model should sufficiently replicate the qualitative aspects of the catalytic system. Missing linker defects may be capped by OH⁻/ H₂O molecules.^{17, 35-37}

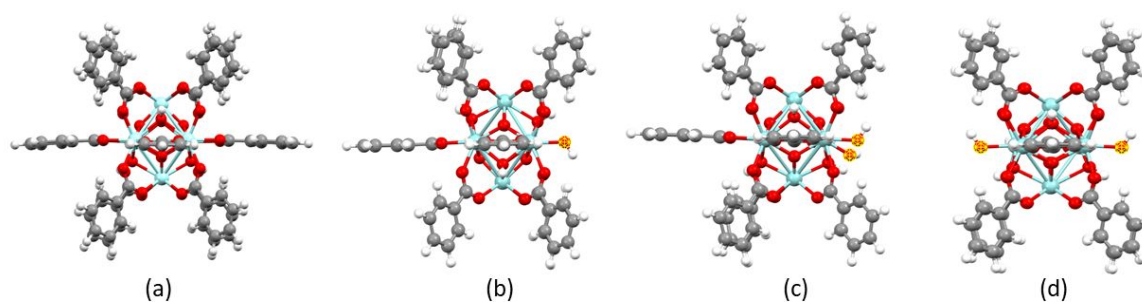


Figure 1. (a) Zirconium node with 12 benzoate linkers. (b) A defective node is created by removing one linker resulting in a Zr-node with 11 linkers. (c) A defective node with two adjacent missing linkers. (d) A defective node with two opposite missing linkers. The carbon atoms furthest away from the Zr-node were constrained in all cases in all directions, to simulate the integrity of the UiO-67 MOF.

With the DFT calculated energetics we constructed a micro kinetic model (MKM) that represents all possible chemical reactions for methanol and water adsorption and desorption. To study the role of water in the transient formation of methanol we performed an isotope study by replacing hydrogen with deuterium in all intermediates and built another MKM as shown in Figure S13 in SI.

Results and Discussion

Characterization

XRD and N₂ adsorption of UiO-67 before and after the BPYDC healing procedure, called UiO-67 and UiO-67(LD), respectively, showed that the procedure had no effect on the crystallinity of the MOF, nor any significant effect on the porosity and surface area of the material (Figure S1 and Figure S2 in SI). This finding suggests that the structural change of the system, if any, is minor.

In line with previous studies of the material, solution state ¹H-NMR analysis identified four organic carboxylate species in both samples; BPDC, BPYDC, benzoic acid (BA) and formic acid (FA), where formic acid originates from decomposition of DMF during synthesis (Figure S3 in SI).³⁸ Quantification of the relative amounts of the species, with respect to BPDC, showed that the BPYDC amount was comparable in the two samples, and in good agreement with the target amount of synthesis (11 and 10 % in UiO-67 and UiO-67(LD), respectively) (Table 1). The benzoic acid amount was 60 % lower in the UiO-67(LD) sample. Thus, successful replacement of a major portion of the benzoic acid in the UiO-67 sample was achieved through the BPDC healing procedure. A minor amount of FA (2 %) was observed in both samples.

Both materials show the same TGA-decomposition profile, but the normalized weight pre-decomposition (T < 500 °C) is significantly higher of the BPDC-healed analog UiO-67(LD), evidencing that the number of Zr-sites coordinated to linker or benzoate is higher as compared to the pristine UiO-67 sample.

Table 1. Solution state ¹H-NMR data of UiO-67 and UiO-67(LD). The amounts are given as percent

Sample	BPYDC	Benzoic acid (BA)	Formic acid (FA)
UiO-67	11	12.5	2.0
UiO-67(LD)	9.9	4.8	1.8

with respect to BPDC.

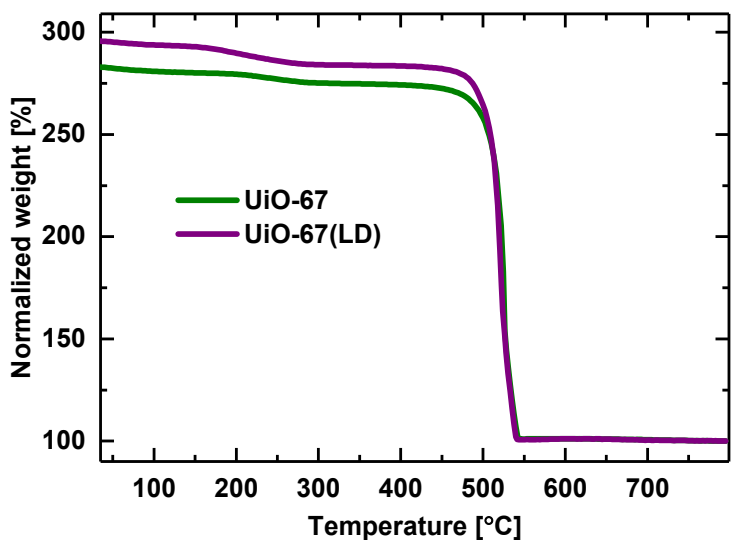


Figure 2. Thermogravimetric analysis of UiO-67 (green) and UiO-67(LD) (purple). The materials were heated at 5 °C min⁻¹ to 800 °C in 25 ml min⁻¹ 20 % O₂/N₂.

Defect calculations³⁹ were performed by combining the results from ¹H-NMR and evaluating the normalized weight during TGA at 200 °C. They showed that BPDC-healing procedure resulted in an increased BPDC: node ratio (increasing from 4.75 to 5.35) and a decreased BA: node ratio (0.68 to 0.27), while the BPYDC and FA to node ratios were unchanged (Table 2). Thus, the parent MOF UiO-67 has, after synthesis, on average one less linker coordinated to each Zr-node, as compared to the healed analog. This translates into one potential active site for methanol formation per node at the Pt-MOF interface,¹⁷ or a total of 660 and 70 μmol open Zr sites per gram of UiO-67 or UiO-67(LD) material, respectively.

Table 2. Defectivity of UiO-67 before and after the BPDC healing procedure, estimated from solution state ¹H-NMR and TGA. The values for each species are per Zr-node. (BPDC+BPYDC): Zr-node

Sample	Wt % _{200 °C}	BPDC	BPYDC	BA	FA
UiO-67	279	4.75	0.59	0.68	0.1
UiO-67(LD)	290	5.35	0.58	0.27	0.1

(cluster) = 6 in the perfect UiO-67 system, each node being coordinated to 12 carboxylate groups.

In our previous work on the UiO-67-Pt material, species originating from benzoate/linkers, as well as residual DMF solvent, were observed in gas phase during the activation procedure at 350 °C in 10 % H₂/Ar.¹⁷ Figure 3 shows the two most intense on-line MS signals related to benzoate/linker type

fragments during activation of UiO-67-Pt and UiO-67(LD)-Pt. The same signal profile is observed for both materials; however, in line with the TGA and $^1\text{H-NMR}$ results, a lower amount of benzoate related species is released from the BPDC-healed sample, UiO-67(LD)-Pt.

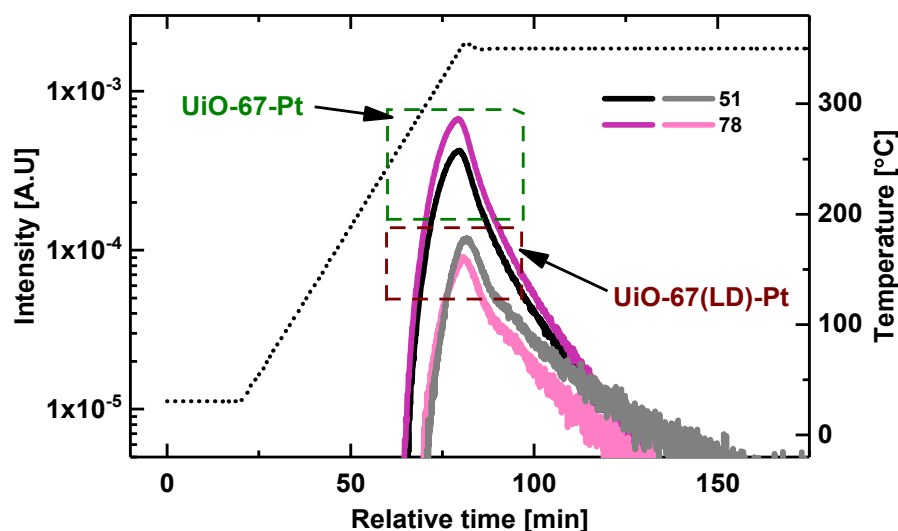


Figure 3. On-line MS signals related to benzoate/linker type fragments during activation of UiO-67-Pt (lilac/black) and UiO-67(LD)-Pt (pink/gray). Conditions: $5\text{ }^{\circ}\text{C min}^{-1}$ ramp to 350°C (4 h dwell) in $20\text{ ml (min}\cdot 0.1\text{g}_{\text{cat}})^{-1}$ flow of 10 % H_2/Ar .

TEM images of UiO-67(LD)-Pt after activation at $350\text{ }^{\circ}\text{C}$ (4 h) followed by testing for CO_2 hydrogenation at $170\text{ }^{\circ}\text{C}$ for ~ 4.5 hours (*vide infra*) are shown in Figure 4. The size of the Pt NPs is around 4 nm in diameter ($3.9 \pm 0.6\text{ nm}$), which is comparable to the non-healed UiO-67-Pt analog ($3.6 \pm 0.7\text{ nm}$, see ref. ¹⁷). Thus, the two catalysts are comparable both in Pt amount and NP size, but differ in the number of Zr node defects, and are therefore suited for investigating the influence of defects on the CO_2 hydrogenation reaction.

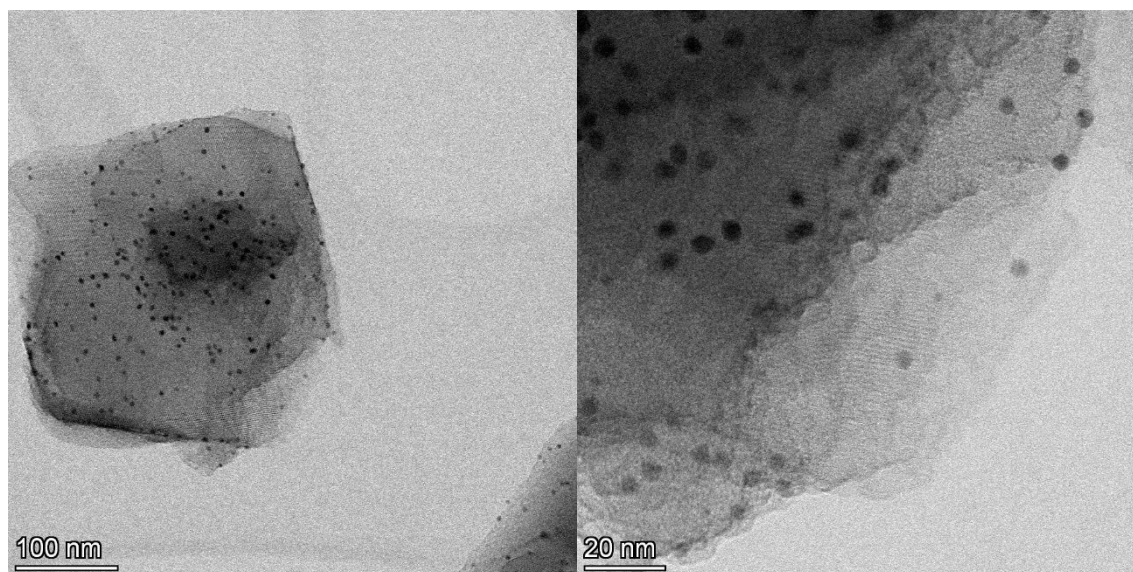


Figure 4. Bright field STEM images of UiO-67(LD)-Pt after activation followed by reaction-onset testing (*vide infra*). See supporting information for instrument details.

An XPS study was carried out for UiO-67 (with 10 % bipy linkers) before and after Pt impregnation, and after subsequent reductive pretreatment as well as catalytic testing (Figure S5-S7 in SI). The study showed that Pt is mainly in reduced state, and that Zr(IV) is partly reduced to Zr(III), after reduction and after subsequent testing of UiO-67-Pt. The results are in agreement with previous XAS studies of UiO-67-Pt and with XPS and NAP-XPS studies of Cu/UiO-66 and CuZn/UiO-67.¹⁴⁻¹⁷

CO₂ adsorption isotherms were measured at 25-50 °C for pristine UiO-67 and for UiO-67-Pt before and after reduction (Figure S8 in SI). Pt impregnation and subsequent reduction led to a small reduction in CO₂ uptake per gram material, but did not change the measured interaction strength between CO₂ and the material. The CO₂ adsorption enthalpy was in all cases 18-19 kJ/mol, similar to what previously reported for UiO-67 MOF.⁴¹

Catalytic Investigation

UiO-67-Pt versus Pt/ZrO₂

Conversion-selectivity plots versus pressure and temperature for UiO-67-Pt and Pt/ZrO₂, obtained under steady-state conditions, clearly demonstrate the superior methanol production ability of the MOF-based catalyst, with a maximum of 42 % (versus 6 %) methanol selectivity at 30 bar, 170 – 190 °C, at similar conversion (Figure 5). This result confirms the unique metal-support interaction created between Pt NPs stabilized by the UiO-67 framework, and the defect (linker-deficient) Zr-nodes surrounding it. The methanol

selectivity observed for the Pt/ZrO₂ catalyst is similar to what was previously reported, i.e.; 6 % methanol selectivity 200 °C, 10 atm.²²

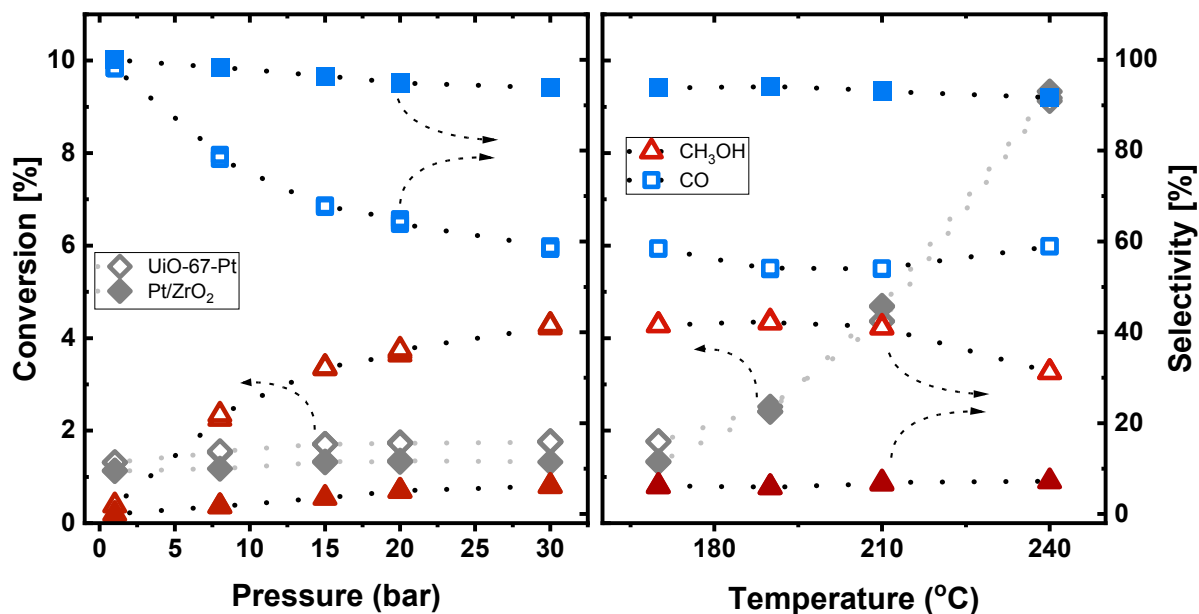


Figure 5. CO₂ conversion (left axes) and product selectivity (right axes) under varying pressure (left graph, T = 170 °C) and temperature (right graph, P_{tot} = 30 bar) conditions over UiO-67-Pt (open symbols) and Pt/ZrO₂ (filled symbols). CO₂ conversion (diamond), CO (square) and CH₃OH (triangle) selectivity. For brevity, the residual selectivity (< 10%) to methane over UiO-67-Pt is not shown. Conditions: CO₂/H₂/inert = 1/6/2, τ = 0.01 g_{UiO-67-Pt}min ml⁻¹, 0.02 g_{Pt/ZrO₂}min ml⁻¹

Influence of Missing Linker Defects on the Reaction

The influence of missing linker defects in UiO-67 (UiO-67-Pt versus UiO-67(LD)-Pt) on catalytic performance was evaluated in a “reaction-onset” experiment by the following procedure: First, the materials were activated in a reducing flow of 10 % H₂ in Ar (40 ml min⁻¹, m_{cat} = 0.2 g, 1 bar) ramping to 350 °C followed by a 4 hour isotherm before cooling to 170 °C in Ar flow. Second, the reaction feed of CO₂/H₂/Ar(10Kr) = 1/3/1, τ = 0.01 g_{cat} min ml⁻¹ was introduced to the reactor and the reactor pressure was subsequently increased to 8 bar. The results are presented in Figure 6, where the formation rates of CO, CH₄ and CH₃OH are shown in the left hand figure, and the CH₃OH selectivity is shown to the right.

Both catalysts show the same trends with time on stream: the rate of methanol formation increases rapidly during the first hour of reaction, then decreases comparatively fast and reaches a steady state after approximately 3 hours on stream. At peak methanol formation, the rate is approximately 6 times higher than at steady state. The formation rates of CO and CH₄ both decrease with time on stream until steady state is reached after about 1.5 hours. The relative temporal change is significantly larger for the small amounts of CH₄ formed, as compared to the majority product CO. Under the given conditions, the CH₄ selectivity was < 1 %. In a second experiment for UiO-67-Pt, where the tested sample was re-activated and re-tested, an identical transient behavior was observed (Figure S9 in SI), suggesting that the transient regime with decreasing activity is caused by reversible catalyst changes. The transient regime of the CO₂ hydrogenation reaction is addressed further in the next section.

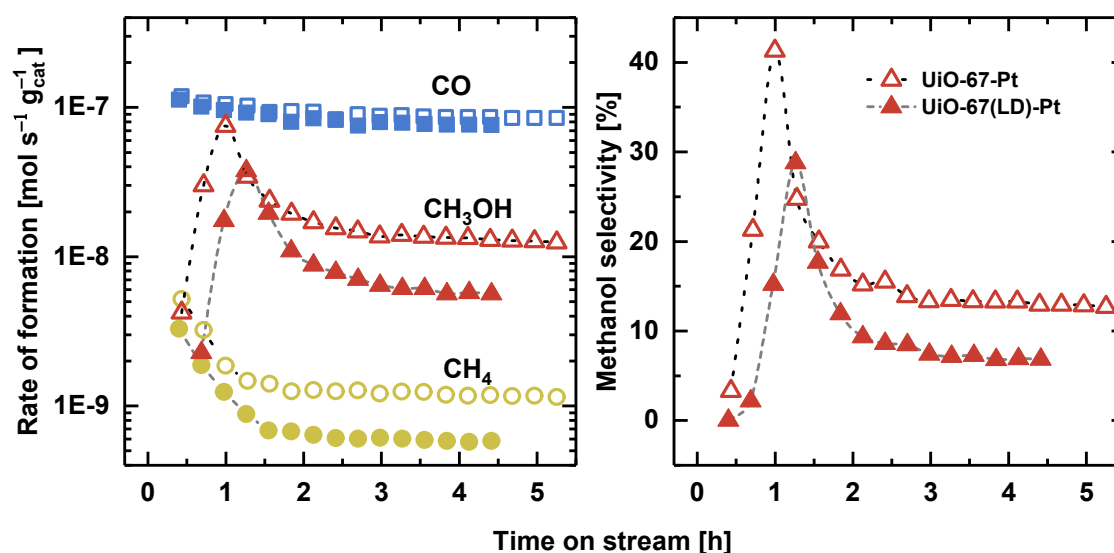


Figure 6. Reaction-onset comparison of UiO-67-Pt (open symbols) and UiO-67(LD)-Pt having intrinsically less benzoic acid modulator (filled symbols). Left: CO (squares), CH₃OH (triangles) and CH₄ (circles) rate of formation. Right: methanol selectivity versus time on stream. Conditions: CO₂/H₂/inert = 1/3/1, $\tau = 0.01 \text{ g}_{\text{cat}} \text{ min ml}^{-1}$, $T = 170 \text{ }^{\circ}\text{C}$, 8 bar.

Comparing the absolute values of the reaction rates over the two catalyst samples, it is evident that the CO formation rates are comparable, while the rate of methanol formation is approximately 60 % lower (at steady state) over the less defective UiO-67(LD)-Pt sample (Figure 6). This corresponds to methanol selectivity of ~7 % and ~13 %, respectively. A 60% decrease was also observed in the methane formation rate, between the UiO-67 and UiO-67(LD) samples. To assess the reproducibility of the measurements, another identical test of UiO-67(LD)-Pt was performed. In that case, the same trend was observed and the methanol formation rate was somewhat higher, yielding a selectivity of ~9 % at steady state, while methane formation rate was the same in both tests (Figure S10 in SI). The

significantly lower activity toward methanol and methane formation over the less defective UiO-67(LD)-Pt sample strongly suggests that a lower number of defects leads to a lower number of active sites for both methanol and methane formation, in turn resulting in a lower rate of formation. This finding is perfectly in line with the postulated mechanism of methanol formation via a formate intermediate bound to open Zr-sites in the Pt NP–MOF interface (see Figure 7).¹⁷ It further suggests that methane is also formed at the interface of the Zr-node and the Pt NP. Conversely, the similar CO formation rates observed over the two materials suggest that the rate-limiting step of CO formation is catalyzed by the Pt NP surface, without an influence of the Pt NP – Zr node interface.

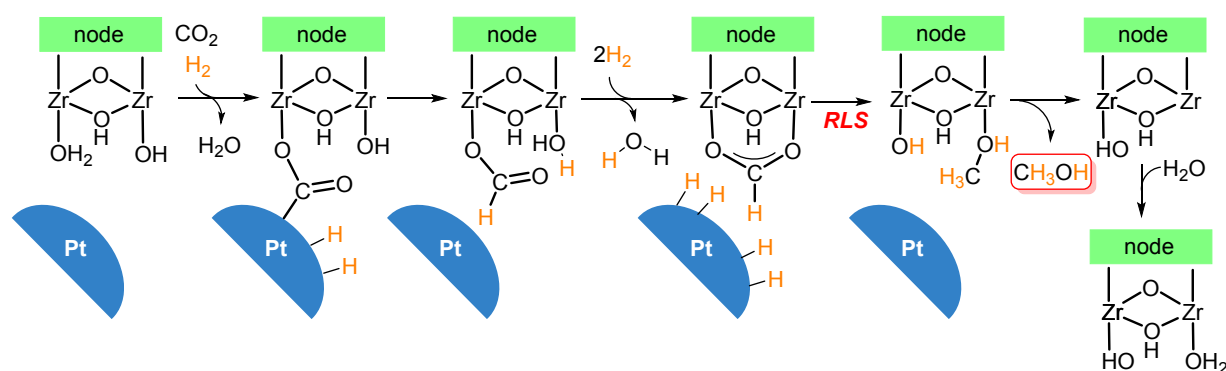


Figure 7. Schematic presentation of the postulated mechanism for methanol formation on an open Zr-site at the UiO-67-Pt Zr-node.

To verify that the origin of the lower methanol and methane formation rates is the number of intermediates, we turned to $^{13}\text{CO}_2$ SSITKA measurements. Due to limitations in the transient experimental set-up, the measurements were performed under ambient pressure. Moreover, the reaction was performed in D_2 instead of H_2 to increase the methanol production (caused by the strong inverse kinetic isotope effect)^{17, 42} and to allow for monitoring of both methanol and methane during the isotope transient. At steady state conditions ($\text{CO}_2/\text{D}_2/\text{inert} = 1/6/3$, $\tau = 0.01 \text{ g}_{\text{cat}} \text{ min ml}^{-1}$, $T = 170^\circ\text{C}$, 1 bar), the rates of CO, methane and methanol formation was approximately 10 %, 60 % and 50 % lower, respectively, over UiO-67(LD)-Pt than over UiO-67-Pt (Figure 8, left), comparable to the differences observed in experiments under 8 bar pressure. The transient evolution of ^{13}CO , $^{13}\text{CD}_4$ and $^{13}\text{CD}_3\text{OD}$ after switching from a feed of $^{13}\text{CO}_2 + \text{D}_2$ to $^{12}\text{CO}_2 + \text{D}_2$ at time = 0, is shown in Figure 8 (right). The transient evolution of the normalized intensity of the ^{13}C products formed over UiO-67(LD)-Pt overlap those of UiO-67-Pt, previously reported in ref. ¹⁷, evidencing that the reaction proceeds through the same mechanism, with the same intrinsic kinetics, while the number of active sites is different.

The mean surface residence time τ_{res} and the number of surface intermediates N_{ad} leading to formation of the three products, listed in Table 3, are parameters where no underlying assumptions

about the kinetic model is required.^{43,44} In agreement with the overlapping isotope transients and the lower steady state methanol formation rate over UiO-67(LD)-Pt (50 % of the rate over UiO-67-Pt), the number of intermediates leading methanol formation on UiO-67(LD)-Pt is 40 % of the number of intermediates on the defective analog. That is, $N_{\text{ad,UiO-67(LD)-Pt}}/N_{\text{ad,UiO-67-Pt}} = 0.4$. A similar observation is made for methane formation, where $N_{\text{ad,UiO-67(LD)-Pt}}/N_{\text{ad,UiO-67-Pt}} = 0.3$. These data confirm the importance of Zr-node defects for methane formation. N_{ad} for CO is on the other hand somewhat lower than expected for the defective analog, since similar reaction rates were observed over the two materials at 8 bar pressure, and only 10% lower CO formation rate was observed here. However, considering the error margins of the experiments and the data treatment, the agreement is reasonable.

As a final observation from the data presented in Figure 8 (right), it is interesting to note that the normalized methanol transients over UiO-67-Pt and UiO-67(LD)-Pt are very similar, in spite of the much higher total number of open Zr sites in UiO-67 (660 $\mu\text{mol/g}$) than in UiO-67(LD) (70 $\mu\text{mol/g}$). This observation suggests that re-adsorption of methanol on open Zr sites downstream of its formation site is kinetically irrelevant.

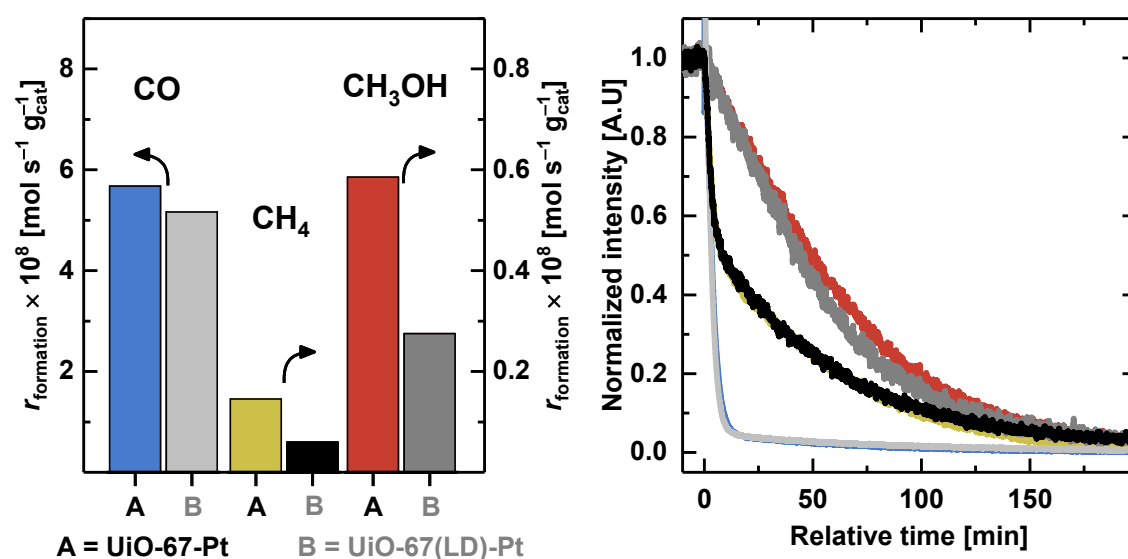


Figure 8. Left: Steady state reaction rates of ¹³CO (blue, light gray), ¹³CD₄ (yellow, black) and ¹³CD₃OD (red, dark gray) over UiO-67-Pt (A, colors) and UiO-67(LD)-Pt (B, gray tones). Right: Transient evolution of the ¹³C-labeled products after switching from ¹³CO₂+D₂ to ¹²CO₂+D₂ at time = 0. ¹³CO, ¹³CD₄ and ¹³CD₃OD are represented by $m/z = 29$, 21 and 35, respectively. Conditions: CO₂/D₂/inert = 1/6/3, $\tau = 0.01 \text{ g}_{\text{cat}} \text{ min ml}^{-1}$, $T = 170 \text{ }^{\circ}\text{C}$, 1 bar.

Table 3. Mean surface residence times τ_{res} and the number N_{ad} of surface intermediates leading to the formation of ^{13}CO , $^{13}\text{CD}_4$ and $^{13}\text{CD}_3\text{OD}$ at 170 °C (1 bar), calculated from integration of the curves and the isotope-independent steady-state reaction rates in Figure 8. Values of τ_{res} are in seconds, and N_{ads} in $\mu\text{mol g}_{\text{cat}}^{-1}$.

	INT(CO)		INT(CD ₄)		INT(CD ₃ OD)	
	τ_{res}	N_{ads}	τ_{res}	N_{ads}	τ_{res}	N_{ads}
UiO-67-Pt	0.5×10^3	26 ± 3	2.1×10^3	3 ± 0.3	3.8×10^3	23 ± 2
UiO-67(LD)-Pt	0.4×10^3	20 ± 3	2.0×10^3	1 ± 0.2	3.3×10^3	9 ± 1

Influence of Zr-Node Hydration on the Reaction

In the comparison of UiO-67-Pt and UiO-67(LD)-Pt, after the onset of reaction at 8 bar pressure, a transient regime lasting approximately 2 hours was observed for the formation of all three carbon-containing reaction products (see Figure 6). In this section, the origin of this transient regime is investigated for UiO-67-Pt.

Upon activating the catalyst for CO₂ hydrogenation (i.e. reduction at 350 °C in 10 % H₂ for 4 hours), the Zr- μ_3 -OH groups of the UiO-67 nodes are completely removed via dehydration.^{45,46} Figure 9 shows an FT-IR spectrum of the Zr- μ_3 -OH region of the sample during activation. The full FT-IR spectrum and its features are described in detail elsewhere.^{17, 45, 47, 48} The intense peak of Zr- μ_3 -OH at 3669 cm⁻¹ decreases with increased temperature, and even before 350 °C is reached, the signal is completely absent. Notably, the dehydration causes a reordering of the Zr-node from Zr₆O₈ (i.e. Zr₆O₄(OH)₄), where Zr is 8-coordinated, to a distorted Zr₆O₆ analog where Zr is 7-coordinated.^{45, 46} The reordering is reversible and does not induce overall changes to the framework structure, nor to the connecting carboxylates.⁴⁵ When the temperature is decreased to 245 °C, and a reaction feed of 1/6 CO₂/H₂ is introduced to the IR-cell, the signal of Zr- μ_3 -OH increases as H₂O is produced in the reaction, and reaches a plateau in less than 5 minutes (Figure 9). At 170°C, under steady state reaction conditions, the signal of Zr- μ_3 -OH is larger, compared to 245 °C. Under these conditions, the Zr- μ_3 -OH groups are dynamic and H readily exchanges for D during H/D exchange experiments, either by direct H-spillover or via reaction products.¹⁷

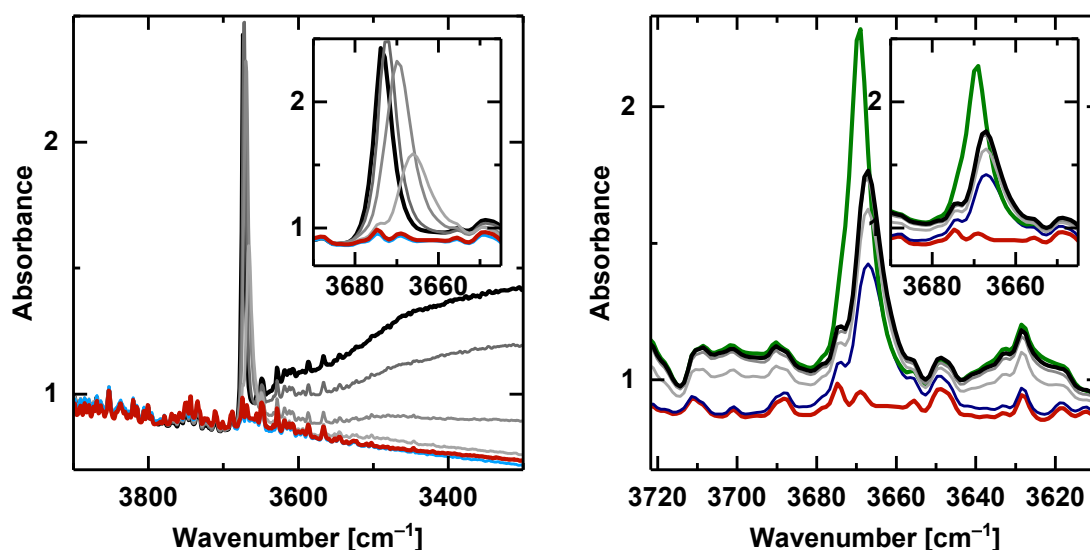


Figure 9. FT-IR spectra of UiO-67-Pt, focusing on Zr- μ_3 -OH. Left: During activation. The black spectrum is collected at room temperature, the gray spectra from darkest to brightest are acquired in 10 min intervals during the temperature ramp to 350 °C (5 °C min⁻¹), and the light blue spectrum is acquired when 350 °C is reached. The red curve is obtained after 4 hours at 350 °C. Right: Red: as in the left figure. Blue: at 245 °C in 10 % H₂, light gray/dark gray/black: 2/3.5/90 min after introducing the reaction feed at 245 °C (CO₂/H₂ = 1/6 ml min⁻¹, 1 bar). Green: after 90 min at 170 °C in reaction feed.

Considering the reaction-onset experiment at 8 bar, we notice that no signal of H₂O was detected in the GC until ~1 hour on stream. Furthermore, the appearance of gas phase H₂O coincided with a substantial drop in the methanol formation rate (Figure 10, left). Interestingly, the molar amount of H₂O formed until it appeared in the GC (calculated from reaction stoichiometry), corresponds to about 40 % of the estimated number of Zr- μ_3 -OH groups in the MOF. This observation indicates a correlation between the transient regime with higher methanol formation rate, and the Zr-nodes' state of hydration and/or the presence of H₂O.

To further investigate the influence of the state of hydration of the Zr-nodes, a reaction-onset experiment was performed starting from a pre-hydrated catalyst. After the activation procedure, the MOF was exposed to a flow of wet Ar (saturated with H₂O vapor at room temperature) at 170 °C prior to the switch to reaction feed and subsequent pressure increase. The product formation rates with time on stream over the initially dehydrated and pre-hydrated catalysts are shown in Figure 10 (right). The transient regime is very different in the two measurements. Over the pre-hydrated catalyst, the methanol peak is gone, and the methanol formation rate instead gradually increases towards steady state, reaching the same value as over the initially dehydrated sample. For methane, the rate of formation starts, and is maintained, at the steady state value, which is the same for the dehydrated and

pre-hydrated catalyst. This observation adds further evidence to the importance of Zr-node defects in CH_4 formation. No evident change in CO formation is observed. The pre-hydration results clearly demonstrate that hydration of the Zr-node is of importance, however, this experiment alone cannot distinguish whether it is due to an intrinsic activity difference between the dehydrated and hydrated Zr-node, or due to competitive adsorption between methanol (and methane) and H_2O . The influence of H_2O on the reaction is addressed further in the following section.

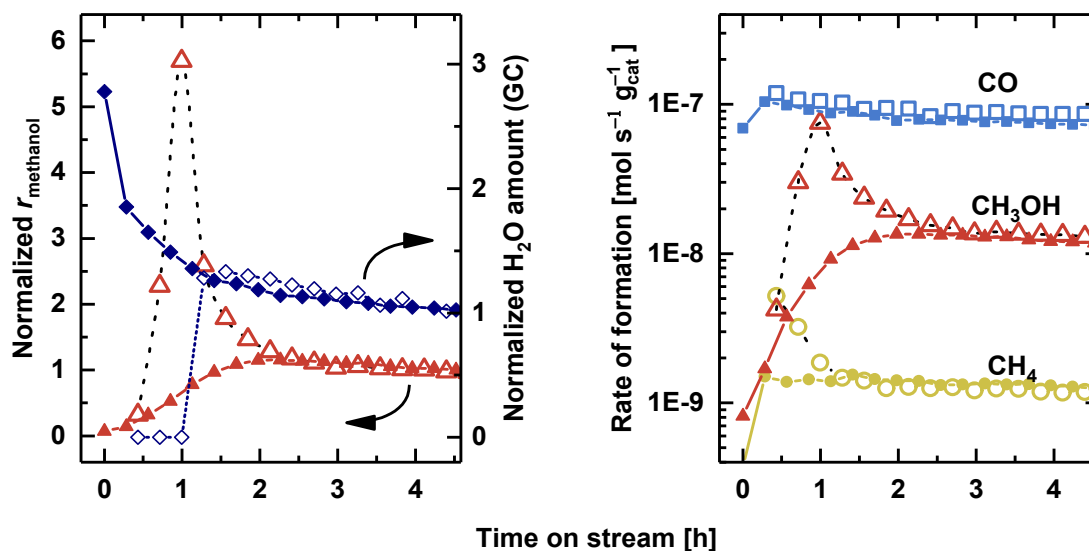


Figure 10. Reaction-onset comparison of the dehydrated (open symbols) and pre-hydrated UiO-67-Pt (small filled). Left: Normalized methanol formation rate (left axis) and steady state normalized H_2O GC amount (diamonds, right axis) versus time on stream. Right: CO (squares), CH_3OH (triangles) and CH_4 (circles) rate of formation. Reaction conditions: $\text{CO}_2/\text{H}_2/\text{inert} = 1/3/1$, $\tau = 0.01 \text{ g}_{\text{cat}} \text{ min ml}^{-1}$, $T = 170 \text{ }^\circ\text{C}$, 8 bar. Pre-hydration: $0.023 \text{ H}_2\text{O}/\text{Ar}$, $\tau = 0.01 \text{ g}_{\text{cat}} \text{ min ml}^{-1}$, $T = 170 \text{ }^\circ\text{C}$, 1 bar.

Influence of H_2O on the Reaction with Hydrated Nodes

The influence of H_2O on the reaction was investigated through co-feed experiments at $170 \text{ }^\circ\text{C}$ and ambient pressure ($\text{CO}_2/\text{H}_2/\text{inert} = 1/6/3$, $\tau = 0.01 \text{ g}_{\text{cat}} \text{ min ml}^{-1}$). To enable monitoring of transient as well as steady state effects, the reaction feed was switched between feeds of CO_2+H_2 and $\text{CO}_2+\text{H}_2+x\text{H}_2\text{O}$ ($x = 0.6, 1.2, 1.7$ and $2 \text{ vol. } \%$). Figure 11 (left) shows the product formation rates when switching from dry to $1.7 \text{ } \%$ H_2O reaction feed. All three carbon-containing products are affected by the presence of H_2O in the reaction feed. The rates of CO and CH_4 formation decrease to a new steady state within the time resolution of the GC measurements (~ 16 minutes), while methanol on the other hand, first increases by more than an order of magnitude then decreases and reaches steady state after ~ 30 minutes.

The influence of pH_2O on the reaction rates at steady state is shown in Figure 11 (right). An increasing H_2O pressure has a substantial inhibiting effect on the CH_4 formation rate (-0.4 order), and

only minor effect on CO formation rate (-0.1 order). In a previous contribution, we reported that all product formation rates decreased with increasing contact time due to an inhibiting effect of CO and/or H₂O.¹⁷ Reaction orders in p(CO+H₂O) of -1.1, -0.7 and -1.0, for CO, CH₄ and CH₃OH formation were observed. Thus, the reaction orders observed here in pH₂O suggest that for CO, self-inhibition mainly causes the negative effect of contact time on the CO formation rate, while both majority products (CO and H₂O) inhibit CH₄ formation, and only CO inhibits CH₃OH formation.

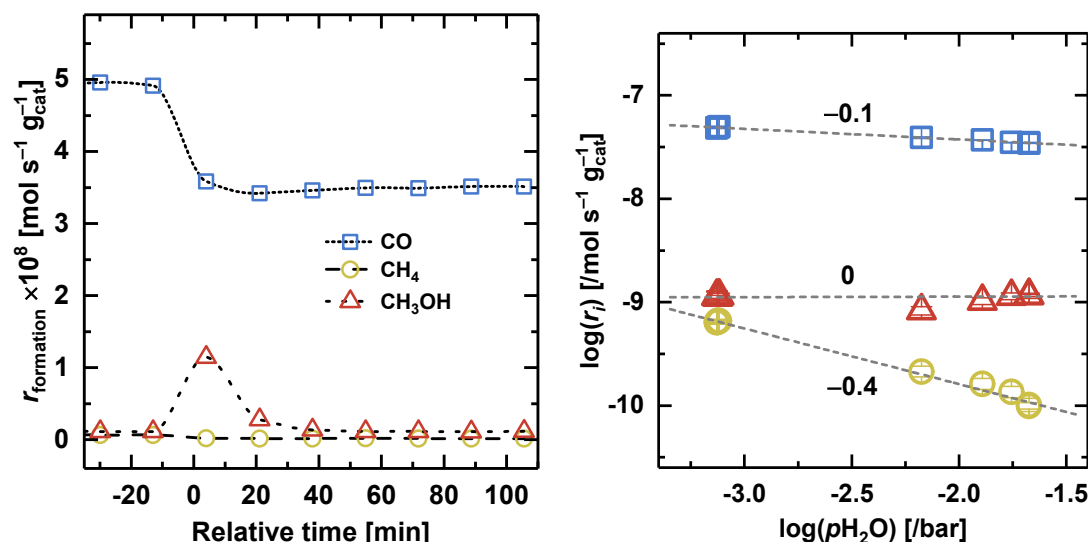


Figure 11. Left: Rate of CO (squares), CH₄ (circles) and CH₃OH (triangles) formation during a switch from CO₂+H₂ to CO₂+H₂+xH₂O ($x = 1.7$ vol. %) at time = 0. Right: Influence of pH₂O on the steady state formation rates of CO, methanol and methane. pH₂O is estimated as the sum of the co-fed pH₂O and half of the pH₂O produced in the reaction at steady state (calculated from reaction stoichiometry). The in-plot numbers are the respective reaction orders. Units in the right-hand figure represent the variable X in “log(X)”. Conditions: CO₂/H₂/inert = 1/6/3 with 0 (yielding an average 0.08), 0.6, 1.2, 1.7 or 2 vol. % H₂O, $\tau = 0.01$ g_{cat} min ml⁻¹, T = 170 °C, 1 bar.

Although a large transient influence of the introduction of H₂O was observed for methanol formation, the steady state value is unchanged (zero order). However, as seen in Figure 11 (right), the rate of methanol formation at pH₂O = 0.006 ($\log(p\text{H}_2\text{O}) = -2.2$) is somewhat lower than the rate under “dry conditions” (i.e. no added H₂O, average $\log(p\text{H}_2\text{O}) = -3.1$), and when the pH₂O increases further, the rate of methanol formation increases slightly (relative to pH₂O = 0.006). When only considering the methanol formation rate under wet conditions in the analysis, the reaction order in pH₂O is estimated to 0.25. If the orders are in fact different at low and high pH₂O, it may suggest that the reaction proceeds via different pathways or is limited by different elementary steps in the two regimes of pH₂O. To assess the possibility of different reaction pathways/rate-limiting steps further, the influence of H₂O should be investigated at pH₂O values closer to those obtained under the “dry”

conditions, as well as in the intermediate range. These pH_2O values are however outside the experimentally achievable range of our test-setup and hence outside the scope of this study.

Having assessed the influence of H_2O at steady state, we turn to the transient influence. Figure 12 (left) shows the intensity of methanol ($m/z = 31$), normalized to the dry steady state reaction rate, when switching from the dry feed to wet feeds containing different pH_2O . The peak size increases significantly with increasing pH_2O in the wet feed, and integration of the peaks yields an approximate 0.5 order dependence in pH_2O for methanol formed during the transient. Interestingly, when switching back from wet to dry conditions, the methanol formation rate instead decreases rapidly, and then slowly increases to the dry steady state value. The normalized intensity of methanol during the switch from 1.7 % to 0 % H_2O in the feed is shown in the inset in Figure 12. Changing from wet to dry conditions, the approach to steady state is somewhat slower, as compared to from dry to wet, but the magnitude of the transient change increases with pH_2O in both cases, i.e. the gas phase methanol concentration decreases with increasing pH_2O . The highly similar, but inverse, behavior of methanol during switches from dry versus wet reaction conditions indicates that the two transients are caused by reversible adsorption/desorption phenomena. Prior studies of other materials showed that methanol may adsorb and form a methoxy group. Water may subsequently react with the methoxy group to re-form gas-phase methanol.⁴⁹⁻⁵³ Such interactions could explain the transient changes in methanol. However, under identical conditions, no methoxy groups were observed during operando FT-IR of UiO-67-Pt.¹⁷ On the other hand, Larmier *et al.* observed methoxy groups on Cu/ZrO_2 by *in situ* DRIFTS when exposed to CO_2 and H_2 (1:3) under 5 bar pressure and 230 °C (closed system), and by *ex situ* solid-state NMR after exposure for 12 hours.¹⁰

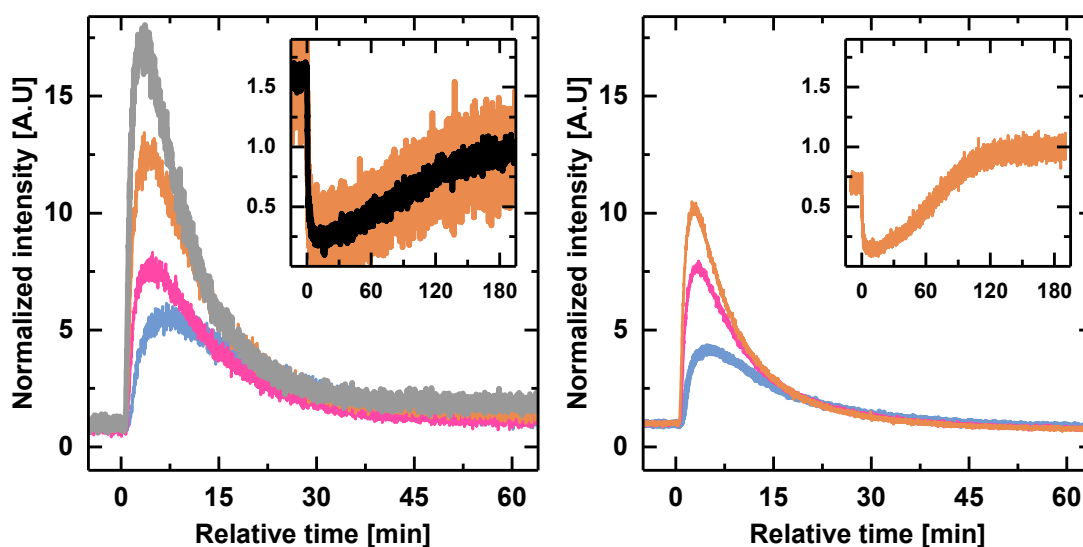


Figure 12. Transient evolution of the normalized methanol formation rate when switching from dry to wet reaction feed, in $\text{CO}_2 + \text{H}_2$ (left) and $\text{CO}_2 + \text{D}_2$ (right). H_2O vol. % in feed = 0.6 (blue), 1.2 (pink),

1.7 (orange) and 2 (gray). The inset shows the rate of methanol formation when switching from wet (1.7 % H₂O) to dry feed. The black trace is a moving average. Conditions: 1/6/3 CO₂/H₂(D₂)/Ar ambient pressure, T = 170 °C, $\tau = 0.01 \text{ g}_{\text{cat}} \text{ min ml}^{-1}$.

To get further insights into the mechanism of transient methanol formation, identical experiments were performed using D₂ instead of H₂, i.e. switching from CO₂+D₂ to CO₂+D₂+xH₂O. By this approach, it is possible to identify the source of hydrogen in the desorbed methanol. At steady state, the influence of pH₂O on the reaction rates in D₂ (Figure 12, right) is unchanged for CO (-0.1) and slightly less negative for methane (-0.3), as compared to H₂. For methanol a negative 0.2 order in pH₂O is observed, and the slope (Figure S11 in SI) is linear in the whole pH₂O range, including dry conditions. Considering the high complexity of the role of H₂O and its influence on the reaction, the origin of this isotope effect is likely manifold.

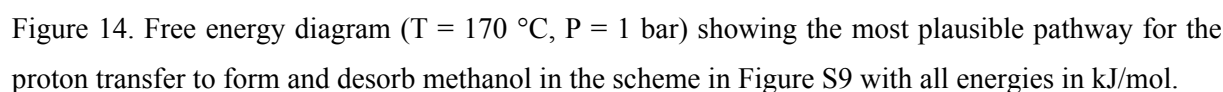
Turning next to the transient regime, Figure 12 (right) shows the intensity of methanol (m/z = 34), normalized to the dry steady state reaction rate, when switching from the dry feed to wet feeds of different pH₂O. The same trend is observed in D₂ as in H₂; the peak size of methanol desorption and adsorption increases with pH₂O. Considering the source of hydrogen, interestingly, the desorbed methanol does not contain significant amounts of H from H₂O. This suggests that methanol desorption via protonation of OCD₃ by H₂O is not the main pathway.

The amount of methanol produced during the transient (in D₂) is approximately 18, 25 and 33 $\mu\text{mol g}_{\text{cat}}^{-1}$ for pH₂O = 0.006, 0.012 and 0.017, respectively. These amounts are comparable to the number of intermediates (23 $\mu\text{mol g}_{\text{cat}}^{-1}$) leading to methanol formation determined from ¹³C-SSITKA under identical, dry, conditions (see Figure 8 and Table 3).

To further understand the role of water in methanol desorption, the free energy pathways for the adsorption of water and methanol to a hydrated Zr-node with one missing linker were calculated at 170 °C (Figure 13 and Table S3 in SI). Starting from the missing linker structure (**1**), which involves two Zr-vacant sites and two μ -O bridges, coordination of water and methanol followed by proton transfer reactions generate the 11 intermediates shown in Figure 13. These intermediates have been labeled by using numbers, to indicate species with different substituents at Zr, and superscript H and/or Me to indicate whether the origin of the substituent is water and/or methanol, respectively. The calculated energy barriers connecting these intermediates are in all cases very low (< 25 kJ/mol for proton transfer reactions and 0 kJ/mol for adsorption of methanol and water in Zr-vacant sites). Therefore, the pathway is mainly dictated by thermodynamics. In the presence of MeOH, the formation of the most stable intermediate **2^{MeMe}**, where methanol is adsorbed on one of the Zr sites (Zr-CH₃OH), methoxy is adsorbed on the other Zr site (Zr-OCH₃) and a proton is adsorbed on one of the μ -O sites (μ -OH), is exergonic by 40.2 kJ/mol. The analogous process with water has a $\Delta G(1 + \text{H}_2\text{O} + \text{H}_2\text{O} \rightarrow 2^{\text{HH}}) = -51.5 \text{ kJ/mol}$, which is 11.3 kJ/mol lower than with methanol. However, in

Figure 13. Free energy pathway ($T = 170\text{ }^{\circ}\text{C}$, $P = 1\text{ bar}$) representing the progression of methanol and water adsorption or proton transfers on a defective Zr-node. Reaction free energies are given between each reaction steps. Energy barriers are shown in parentheses. Red arrows represent the preferred pathway for reactions involving only MeOH, blue arrows for reactions involving only water, and green arrows for reactions involving water and methanol. All energies are in kJ/mol.

As discussed above (Figure 12), co-feed experiments shows that adding water into the system increases the observed methanol concentration initially. To gain further insight into this experimental observation, we set up a MKM where the equilibrated structure 2^{MeH} at 1 mol/l concentration was used as a starting point and then different amounts of water is introduced to the system (see Figure S12 in SI). These simulations show that when any additional water was introduced into the system it causes methanol to desorb from the system, in agreement with the experimental observations. The adsorbed methanol is desorbed from the Zr-site and is replaced by a water molecule, resulting in structure 2^{HH} in Figure 13. The equilibria $2^{\text{MeH}} \leftrightarrow 3^{\text{H}} \leftrightarrow 2^{\text{HH}}$ is in agreement with the non-observation of CD_3OH in the experiments performed with CO_2 and D_2 followed by addition of H_2O (see Figure 7, in which the orange H could be D). However, the equilibria between 2^{MeH} and 3^{Me} , which is thermodynamically preferred, could also play a role in the reaction leading to H/D-exchange. To determine the relevance of this process, DFT calculations were performed considering deuterated species and different proton-transfer mechanisms (Figure 14 and Figure S13). All mechanisms proceed without any additional energy barriers beyond thermodynamics. Figure 14 shows that the relative energy of $3^{\text{H-H}}$ compared to $2^{\text{CD}_3\text{-D-D}}$ ($\Delta G = 34.3\text{ kJ/mol}$) decreases significantly compared to the analogous intermediates without – D (3^{H} and 2^{MeH} , $\Delta G = 50.4\text{ kJ/mol}$, in Figure 13). In addition, intermediate $2^{\text{H-H-H}}$ becomes the most preferred intermediate compared to $2^{\text{CD}_3\text{-D-D}}$, $2^{\text{CD}_3\text{-H-D}}$ or $2^{\text{CD}_3\text{-H-H}}$, favoring the desorption of CD_3OD (see Table S4). Nevertheless, these energy differences are created because of the isotope exchange, and will not exist in a normal experiment using H_2 , in which the proton in desorbed methanol may originate from either water already present or newly added.



22

adjacent linkers, the adsorption energies change drastically, especially in the case where water is coordinated to one Zr-atom attached to an OH group ($\Delta G = + 66.9$ kJ/mol). This result strongly suggests that having a larger number of defects not only increases the number of active sites to produce methanol but also facilitates methanol desorption.

These results show that both water and missing linkers play an important role in methanol desorption by either displacing the equilibria or changing the methanol adsorption energies. However, Figure 10 suggests that water does not have an important influence on the MeOH formation rate at steady state. Instead, it decreases the rate of methane significantly. An explanation to this observation is the following: As represented in Figure 15, interaction of adsorbed CO with a Zr atom from a node should be feasible at the interface between Pt NPs and Zr nodes. This coordination would increase the electrophilicity of C and favor the hydride transfer, which has been proposed to be the rate-limiting step for the CO hydrogenation to methane with Pt-NPs.⁵⁸ When adding water to the system, the equilibria between CO and water will be displaced favoring water coordination and disfavoring methane formation. In the case of methanol (see Figure 7), this competition takes place before the formation of formate, which is thermodynamically preferred of having **2^{HII}**. Therefore, it would not influence the rate-limiting step of methanol, which has been proposed to be the hydrogenation of formate.

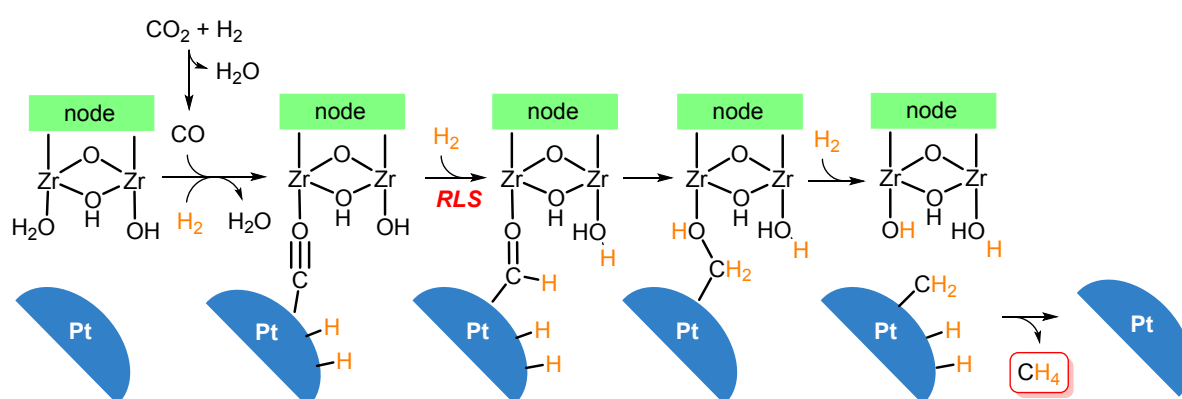


Figure 15. Schematic presentation of the postulated mechanism for the methane formation on an open Zr-site at the UiO-67-Pt Zr-node.

Conclusions

The dynamic role of the Zr-node during CO₂ hydrogenation over UiO-67-Pt and the influence of defects and water on the reaction have been investigated by steady state and isotope transient kinetic studies, as well as water co-feed experiments.

A UiO-67-Pt MOF catalyst was designed with less defects to influence the rate of methanol formation. ¹³C-SSITKA experiments verified that a lower number of defect sites led to lower methanol formation rates, and that this decrease was caused by a lower number of surface intermediates. This

1
2
3 result serves as a proof-of-principle in rational design of a MOF catalyst based on fundamental
4 understanding. Importantly, the methane formation rate had a similar dependency of Zr node defects,
5 while the CO formation rate was almost invariant with defect density. These results strongly suggest
6 that the rate-limiting step of CO formation occurs at the Pt NPs, while the rate-limiting step of
7 methane formation, like methanol, takes place at the Pt NP-Zr node interface.
8
9

10
11 By comparing the onset of reaction over a sample with dehydrated Zr-nodes to the onset over
12 a pre-hydrated sample, it was found that the rate of methanol and methane formation are both higher
13 over a dehydrated node than over a hydrated node. Adding surplus water to the feed has an inhibiting
14 effect on methane formation, but not on methanol formation, suggesting that methanol selectivity may
15 be optimized by steam addition to the reactant gas feed. Moreover, transient H₂O co-feed experiments
16 showed that the introduction of H₂O causes substantial amounts of methanol to desorb from the
17 catalyst; while removal of H₂O causes re-adsorption. No transfer of hydrogen from H₂O to the
18 desorbed methanol was observed, suggesting that the cause of desorption is competitive adsorption.
19 DFT calculations showed that methanol is adsorbed weaker on less hydrated and more defective
20 nodes, which can contribute to the observation of larger amounts of methanol with these systems.
21
22
23
24
25
26
27
28
29

30 Supporting Information

31
32 XRD, N₂ adsorption isotherms, solution state NMR, STEM, additional catalytic test data,
33 XPS, CO₂ adsorption isotherms, computational details, geometries for all computed
34 structures (xyz file) and additional computational data.
35
36
37
38
39
40

41 Acknowledgement

42 E.S.G, G.K., A.L., S.S. and U.O. acknowledge the Research Council of Norway for financial support
43 (FRINATEK ToppForsk Grant No. 250795 CONFINE). H.P., E.S. and A.N. acknowledge
44 support by the 'Nordic Consortium for CO₂ Conversion' (NordForsk project No.
45 85378, site.uit.no/nordco2) and the Norwegian Metacenter for Computational Science
46 (NOTUR) for computational resources (project number nn4654k). A. N. acknowledge the
47 support from the Research Council of Norway (FRINATEK Grant No. 250044 and Center of
48 Excellence Grant No. 262695). B.G.S. and A.E.G. acknowledge the Research Council of
49 Norway for its support of the Norwegian Center for Transmission Electron Microscopy
50 (NORTEM) (197405/F50).
51
52
53
54
55
56
57
58
59
60

1
2
3 **Author Information**
4 **Corresponding Author**
5
6 *unni.olsbye@kjemi.uio.no
7
8 *ainara.nova@kjemi.uio.no
9

10
11
12
13
14
15
16
17
18
19
20
21
22
23
24
25
26
27
28
29
30
31
32
33
34
35
36
37
38
39
40
41
42
43
44
45
46
47
48
49
50
51
52
53
54
55
56
57
58
59
60

Reference

1. Aresta, M.; Dibenedetto, A.; Angelini, A., The changing paradigm in CO₂ utilization. *J. CO₂ Util.* **2013**, 3-4, 65-73.
2. Olah, G. A., Beyond Oil and Gas: The Methanol Economy. *Angew. Chem. Int. Ed.* **2005**, 44 (18), 2636-2639.
3. Matzen, M.; Demirel, Y., Methanol and dimethyl ether from renewable hydrogen and carbon dioxide: Alternative fuels production and life-cycle assessment. *J. Cleaner Prod.* **2016**, 139, 1068-1077.
4. Kattel, S.; Liu, P.; Chen, J. G., Tuning Selectivity of CO₂ Hydrogenation Reactions at the Metal/Oxide Interface. *J. Am. Chem. Soc.* **2017**, 139 (29), 9739-9754.
5. Li, K.; Chen, J. G., CO₂ Hydrogenation to Methanol over ZrO₂-Containing Catalysts: Insights into ZrO₂ Induced Synergy. *ACS Catal.* **2019**, 9 (9), 7840-7861.
6. Meunier, F. C., Mixing Copper Nanoparticles and ZnO Nanocrystals: A Route towards Understanding the Hydrogenation of CO₂ to Methanol? *Angew. Chem. Int. Ed.* **2011**, 50 (18), 4053-4054.
7. Rodriguez, J. A.; Liu, P.; Stacchiola, D. J.; Senanayake, S. D.; White, M. G.; Chen, J. G., Hydrogenation of CO₂ to Methanol: Importance of Metal–Oxide and Metal–Carbide Interfaces in the Activation of CO₂. *ACS Catal.* **2015**, 5 (11), 6696-6706.
8. Roy, S.; Cherevotan, A.; Peter, S. C., Thermochemical CO₂ Hydrogenation to Single Carbon Products: Scientific and Technological Challenges. *ACS Energy Lett.* **2018**, 3 (8), 1938-1966.
9. Lam, E.; Larmier, K.; Wolf, P.; Tada, S.; Safonova, O. V.; Copéret, C., Isolated Zr Surface Sites on Silica Promote Hydrogenation of CO₂ to CH₃OH in Supported Cu Catalysts. *J. Am. Chem. Soc.* **2018**, 140 (33), 10530-10535.
10. Larmier, K.; Liao, W.-C.; Tada, S.; Lam, E.; Verel, R.; Bansode, A.; Urakawa, A.; Comas-Vives, A.; Copéret, C., CO₂-to-Methanol Hydrogenation on Zirconia-Supported Copper Nanoparticles: Reaction Intermediates and the Role of the Metal–Support Interface. *Angew. Chem. Int. Ed.* **2017**, 56 (9), 2318-2323.
11. Lam, E.; Larmier, K.; Tada, S.; Wolf, P.; Safonova, O. V.; Copéret, C., Zr(IV) surface sites determine CH₃OH formation rate on Cu/ZrO₂/SiO₂ - CO₂ hydrogenation catalysts. *Chin. J. Catal.* **2019**, 40 (11), 1741-1748.
12. Lam, E.; Corral-Pérez, J. J.; Larmier, K.; Noh, G.; Wolf, P.; Comas-Vives, A.; Urakawa, A.; Copéret, C., CO₂ Hydrogenation on Cu/Al₂O₃: Role of the Metal/Support Interface in Driving Activity and Selectivity of a Bifunctional Catalyst. *Angew. Chem.* **2019**, 131 (39), 14127-14134.
13. Ferri, D.; Burgi, T.; Baiker, A., Probing boundary sites on a Pt/Al₂O₃ model catalyst by CO₂ hydrogenation and in situ ATR-IR spectroscopy of catalytic solid-liquid interfaces. *Phys. Chem. Chem. Phys.* **2002**, 4 (12), 2667-2672.
14. Rungtaweeveranit, B.; Baek, J.; Araujo, J. R.; Archanjo, B. S.; Choi, K. M.; Yaghi, O. M.; Somorjai, G. A., Copper Nanocrystals Encapsulated in Zr-based Metal–Organic Frameworks for Highly Selective CO₂ Hydrogenation to Methanol. *Nano Lett* **2016**, 16 (12), 7645-7649.
15. An, B.; Zhang, J.; Cheng, K.; Ji, P.; Wang, C.; Lin, W., Confinement of Ultrasmall Cu/ZnOx Nanoparticles in Metal–Organic Frameworks for Selective Methanol Synthesis from Catalytic Hydrogenation of CO₂. *J. Am. Chem. Soc.* **2017**, 139 (10), 3834-3840.
16. Gutterød, E. S.; Øien-Ødegaard, S.; Bossers, K.; Nieuwelink, A.-E.; Manzoli, M.; Braglia, L.; Lazzarini, A.; Borfecchia, E.; Ahmadigoltapeh, S.; Bouchevreau, B.; Lønstad-Bleken, B. T.; Henry, R.; Lamberti, C.; Bordiga, S.; Weckhuysen, B. M.; Lillerud, K. P.; Olsbye, U., CO₂ Hydrogenation over Pt-Containing UiO-67 Zr-MOFs—The Base Case. *Ind. Eng. Chem. Res.* **2017**, 56 (45), 13206-13218.
17. Gutterød, E. S.; Lazzarini, A.; Fjermestad, T.; Kaur, G.; Manzoli, M.; Bordiga, S.; Svelle, S.; Lillerud, K. P.; Skulason, E.; Øien-Ødegaard, S.; Nova, A.; Olsbye, U., Hydrogenation of CO₂ to Methanol by Pt Nanoparticles Encapsulated in UiO-67: Deciphering the Role of the MOF. *J. Am. Chem. Soc.* **2020**, 142 (2), 999–1009.

18. Li, X.; Liu, G.; Xu, D.; Hong, X.; Edman Tsang, S. C., Confinement of subnanometric PdZn at a defect enriched ZnO/ZIF-8 interface for efficient and selective CO₂ hydrogenation to methanol. *J. Mater. Chem. A* **2019**, 7 (41), 23878-23885.
19. Gutov, O. V.; Hevia, M. G.; Escudero-Adán, E. C.; Shafir, A., Metal–Organic Framework (MOF) Defects under Control: Insights into the Missing Linker Sites and Their Implication in the Reactivity of Zirconium-Based Frameworks. *Inorg. Chem.* **2015**, 54 (17), 8396-8400.
20. Braglia, L.; Borfecchia, E.; Lomachenko, K. A.; Bugaev, A. L.; Guda, A. A.; Soldatov, A. V.; Bleken, B. T. L.; Øien-Ødegaard, S.; Olsbye, U.; Lillerud, K. P.; Bordiga, S.; Agostini, G.; Manzoli, M.; Lamberti, C., Tuning Pt and Cu sites population inside functionalized UiO-67 MOF by controlling activation conditions. *Faraday Discuss.* **2017**, 201 (0), 265-286.
21. Øien, S.; Agostini, G.; Svelle, S.; Borfecchia, E.; Lomachenko, K. A.; Mino, L.; Gallo, E.; Bordiga, S.; Olsbye, U.; Lillerud, K. P.; Lamberti, C., Probing Reactive Platinum Sites in UiO-67 Zirconium Metal–Organic Frameworks. *Chem. Mater.* **2015**, 27 (3), 1042-1056.
22. Inoue, T.; Iizuka, T., Hydrogenation of carbon dioxide and carbon monoxide over supported platinum catalysts, *J. Chem. Soc., Faraday Transactions* **1985**, 82 (6), 1681-1686.
23. VandeVondele, J.; Krack, M.; Mohamed, F.; Parrinello, M.; Chassaing, T.; Hutter, J., Quickstep: Fast and accurate density functional calculations using a mixed Gaussian and plane waves approach. *Computer Physics Communications* **2005**, 167 (2), 103-128.
24. Lippert, B. G.; Parrinello, J. H.; Michele, A hybrid Gaussian and plane wave density functional scheme. *Molecular Physics* **1997**, 92 (3), 477-488.
25. Lippert, G.; Hutter, J.; Parrinello, M., The Gaussian and augmented-plane-wave density functional method for ab initio molecular dynamics simulations. *Theoretical Chemistry Accounts* **1999**, 103 (2), 124-140.
26. Genovese, L.; Deutsch, T.; Neelov, A.; Goedecker, S.; Beylkin, G., Efficient solution of Poisson's equation with free boundary conditions. *The Journal of Chemical Physics* **2006**, 125 (7), 074105.
27. Marek, A.; Blum, V.; Johanni, R.; Havu, V.; Lang, B.; Auckenthaler, T.; Heinecke, A.; Bungartz, H.-J.; Lederer, H., The ELPA library: scalable parallel eigenvalue solutions for electronic structure theory and computational science. *Journal of Physics: Condensed Matter* **2014**, 26 (21), 213201.
28. Perdew, J. P.; Burke, K.; Ernzerhof, M., Generalized Gradient Approximation Made Simple. *Physical Review Letters* **1996**, 77 (18), 3865-3868.
29. Grimme, S.; Ehrlich, S.; Goerigk, L., Effect of the damping function in dispersion corrected density functional theory. *Journal of Computational Chemistry* **2011**, 32 (7), 1456-1465.
30. Goedecker, S.; Teter, M.; Hutter, J., Separable dual-space Gaussian pseudopotentials. *Physical Review B* **1996**, 54 (3), 1703-1710.
31. Krack, M., Pseudopotentials for H to Kr optimized for gradient-corrected exchange-correlation functionals. *Theoretical Chemistry Accounts* **2005**, 114 (1), 145-152.
32. Henkelman, G.; Jónsson, H., Improved tangent estimate in the nudged elastic band method for finding minimum energy paths and saddle points. *The Journal of Chemical Physics* **2000**, 113 (22), 9978-9985.
33. Henkelman, G.; Uberuaga, B. P.; Jónsson, H., A climbing image nudged elastic band method for finding saddle points and minimum energy paths. *The Journal of Chemical Physics* **2000**, 113 (22), 9901-9904.
34. Hoops, S.; Sahle, S.; Gauges, R.; Lee, C.; Pahle, J.; Simus, N.; Singhal, M.; Xu, L.; Mendes, P.; Kummer, U., COPASI—a COMplex PATHway Simulator. *Bioinformatics* **2006**, 22 (24), 3067-3074.
35. Øien, S.; Wragg, D.; Reinsch, H.; Svelle, S.; Bordiga, S.; Lamberti, C.; Lillerud, K. P., Detailed structure analysis of atomic positions and defects in zirconium metal–organic frameworks. *Crystal growth & design* **2014**, 14 (11), 5370-5372.
36. Trickett, C. A.; Gagnon, K. J.; Lee, S.; Gándara, F.; Bürgi, H. B.; Yaghi, O. M., Definitive molecular level characterization of defects in UiO-66 crystals. *Angewandte Chemie International Edition* **2015**, 54 (38), 11162-11167.

37. Shearer, G. C.; Chavan, S.; Ethiraj, J.; Vitillo, J. G.; Svelle, S.; Olsbye, U.; Lamberti, C.; Bordiga, S.; Lillerud, K. P., Tuned to perfection: ironing out the defects in metal–organic framework UiO-66. *Chemistry of Materials* **2014**, *26* (14), 4068-4071.
38. Yang, D.; Ortuño, M. A.; Bernales, V.; Cramer, C. J.; Gagliardi, L.; Gates, B. C., Structure and dynamics of Zr6O8 metal–organic framework node surfaces probed with ethanol dehydration as a catalytic test reaction. *Journal of the American Chemical Society* **2018**, *140* (10), 3751-3759.
39. Shearer, G. C.; Chavan, S.; Bordiga, S.; Svelle, S.; Olsbye, U.; Lillerud, K. P., Defect Engineering: Tuning the Porosity and Composition of the Metal–Organic Framework UiO-66 via Modulated Synthesis. *Chem. Mater.* **2016**, *28* (11), 3749-3761.
40. Kaur, G.; Øien-Ødegaard, S.; Lazzarini, A.; Chavan, S. M.; Bordiga, S.; Lillerud, K. P.; Olsbye, U., Controlling the Synthesis of Metal–Organic Framework UiO-67 by Tuning Its Kinetic Driving Force. *Cryst. Growth Des.* **2019**, *19* (8), 4246-4251.
41. Øien-Ødegaard, S.; Bouchevreau, B.; Hylland, K.; Wu, L.; Blom, R.; Grande, C.; Olsbye, U.; Tilset, M.; Lillerud, K.P., UiO-67-type Metal–Organic Frameworks with Enhanced Water Stability and Methane Adsorption Capacity. *Inorganic Chemistry* **2016**, *55* (5), 1986–1991.
42. Kunkes, E. L.; Studt, F.; Abild-Pedersen, F.; Schlögl, R.; Behrens, M., Hydrogenation of CO₂ to methanol and CO on Cu/ZnO/Al₂O₃: Is there a common intermediate or not? *J. Catal.* **2015**, *328*, 43-48.
43. Ledesma, C.; Yang, J.; Chen, D.; Holmen, A., Recent Approaches in Mechanistic and Kinetic Studies of Catalytic Reactions Using SSITKA Technique. *ACS Catal.* **2014**, *4* (12), 4527-4547.
44. Shannon, S. L.; Goodwin, J. G., Characterization of Catalytic Surfaces by Isotopic-Transient Kinetics during Steady-State Reaction. *Chem. Rev.* **1995**, *95* (3), 677-695.
45. Cavka, J. H.; Jakobsen, S.; Olsbye, U.; Guillou, N.; Lamberti, C.; Bordiga, S.; Lillerud, K. P., A New Zirconium Inorganic Building Brick Forming Metal Organic Frameworks with Exceptional Stability. *J. Am. Chem. Soc.* **2008**, *130* (42), 13850-13851.
46. Valenzano, L.; Civalleri, B.; Chavan, S.; Bordiga, S.; Nilsen, M. H.; Jakobsen, S.; Lillerud, K. P.; Lamberti, C., Disclosing the Complex Structure of UiO-66 Metal Organic Framework: A Synergic Combination of Experiment and Theory. *Chem. Mater.* **2011**, *23* (7), 1700-1718.
47. Chavan, S.; Vitillo, J. G.; Gianolio, D.; Zavorotynska, O.; Civalleri, B.; Jakobsen, S.; Nilsen, M. H.; Valenzano, L.; Lamberti, C.; Lillerud, K. P.; Bordiga, S., H₂storage in isostructural UiO-67 and UiO-66 MOFs. *Phys. Chem. Chem. Phys.* **2012**, *14* (5), 1614-1626.
48. Shearer, G. C.; Forselv, S.; Chavan, S.; Bordiga, S.; Mathisen, K.; Bjørgen, M.; Svelle, S.; Lillerud, K. P., In Situ Infrared Spectroscopic and Gravimetric Characterisation of the Solvent Removal and Dehydroxylation of the Metal Organic Frameworks UiO-66 and UiO-67. *Top. Catal.* **2013**, *56* (9), 770-782.
49. Dyballa, M.; Thorshaug, K.; Pappas, D. K.; Borfecchia, E.; Kvande, K.; Bordiga, S.; Berlier, G.; Lazzarini, A.; Olsbye, U.; Beato, P.; Svelle, S.; Arstad, B., Zeolite Surface Methoxy Groups as Key Intermediates in the Stepwise Conversion of Methane to Methanol. *ChemCatChem* **2019**, *11* (20), 5022-5026.
50. Edwards, J. F.; Schrader, G. L., Methanol, formaldehyde, and formic acid adsorption on methanol synthesis catalysts. *J. Phys. Chem.* **1985**, *89* (5), 782-788.
51. Pelmenchikov, A. G.; Morosi, G.; Gamba, A.; Zecchina, A.; Bordiga, S.; Paukshitis, E. A., Mechanisms of methanol adsorption on silicalite and silica: IR spectra and ab-initio calculations. *J. Phys. Chem.* **1993**, *97* (46), 11979-11986.
52. Wang, Z.; Xiong, F.; Sun, G.; Jin, Y.; Huang, W., Structural Dependence of Competitive Adsorption of Water and Methanol on TiO₂ Surfaces. *Chin. J. Chem.* **2017**, *35* (6), 889-895.
53. Alayon, E. M.; Nachtegaal, M.; Ranocchiari, M.; van Bokhoven, J. A., Catalytic conversion of methane to methanol over Cu-mordenite. *Chem. Commun.* **2012**, *48* (3), 404-406.
54. A proton transfer from the adsorbed OH₂ to OCH₃ is observed during geometry optimization
55. Yang, D.; Gaggioli, C. A.; Ray, D.; Babucci, M.; Gagliardi, L.; Gates, B. C., Tuning Catalytic Sites on Zr₆O₈ Metal–Organic Framework Nodes via Ligand and Defect Chemistry Probed with tert-Butyl Alcohol Dehydration to Isobutylene. *J. Am. Chem. Soc.* **2020**, *142* (17), 8044-8056.

1
2
3
4
5
6
7
8
9
10
11
12
13
14
15
16
17
18
19
20
21
22
23
24
25
26
27
28
29
30
31
32
33
34
35
36
37
38
39
40
41
42
43
44
45
46
47
48
49
50
51
52
53
54
55
56
57
58
59
60

56. Vandichel, M.; Hajek, J.; Ghysels, A.; De Vos, A.; Waroquier, M.; Van Speybroeck, V., Water coordination and dehydration processes in defective UiO-66 type metal organic frameworks. *CrystEngComm* **2016**, *18* (37), 7056-7069.

57. Caratelli, C.; Hajek, J.; Cirujano, F. G.; Waroquier, M.; i Xamena, F. X. L.; Van Speybroeck, V., Nature of active sites on UiO-66 and beneficial influence of water in the catalysis of Fischer esterification. *Journal of catalysis* **2017**, *352*, 401-414.

58. Kattel, S.; Yan, B.; Chen, J. G.; Liu, P., CO2 hydrogenation on Pt, Pt/SiO2 and Pt/TiO2: Importance of synergy between Pt and oxide support. *Journal of Catalysis* **2016**, *343*, 115-126.

For Table of Contents Only

